small NANO MICRO

Lithography

DOI: 10.1002/smll.200700859

Positive and Negative ZnO Micropatterning on Functionalized Polymer Surfaces**

*Peng Yang, Shengli Zou, and Wantai Yang**

Patterned ZnO deposition on substrates has received increasing attention because of its great potential in photocatalysis, energy conversion, and electro-optical techniques. Chemical solution growth is especially promising for organic substrates due to its very mild reaction conditions. Here this method is used on functionality-patterned polymer surfaces in order to fabricate positive and negative ZnO micropatterns. A ZnO film made of arrayed rods, typically 500–750 nm in diameter and 2.5 μm in length, is selectively obtained on sulfated and hydroxylated regions of biaxially oriented poly(propylene), giving rise to positive patterns. For reactive polyesters such as poly(ethylene terephthalate), the ZnO rods selectively remain on the unmodified original regions, creating negative patterns. Unlike complex photolithography procedures, the irradiation and patterning processes do not require the use of positive or negative photoresists, and possible damage from acidic solutions on the underlying substrate during the chemical etching process is avoided. The process thus proves to be a simple, creditable, and low-cost method, which could be easily applied on a variety of inert and reactive polymer surfaces.

Keywords:
- lithography
- patterning
- polymers
- semiconductors
- surfaces

1. Introduction

Zinc oxide is an interesting choice as a semiconductor material due to its great potential in solar cells,[1] sensors,[2] optical storage,[3] transistors,[4] catalysis,[5] UV protection,[6] and light-emitting materials.[7] With the exception of self-standing films, ZnO films require a support and, up until now, most of these consist of metal and inorganic substrates. However, fast development of flexible and light devices draws increasing attention to flexible organic polymer substrates.[8]

The patterning or array of ZnO nanostructures on substrates is often necessary when producing controllable and designable devices. The methods for fabricating such patterns can be categorized into the following four protocols: 1) templating,[9] 2) direct etching or photolithography,[10–15] 3) patterning catalysis and the consequent in situ catalyzed ZnO growth,[16–21] and 4) aqueous chemical growth (ACG)[22–26] or atomic layer epitaxy (ALE)[27] on surfaces modified by hybrid self-assembly monolayers (SAMs). For weaker and dielectric plastic substrates, not all of the above methods are suitable since mild fabrication conditions, such as a low handling temperature and little damage to the substrates, are strong issues. Etching is usually performed on substrates after ACG to produce desired patterns. Kreye et al.[10] have generated patterned arrays of ZnO nanorods on the micrometer-scale on poly(ethylene naphthalate) (PEN) surfaces by a lithographic (wet acidic etching) technique. Chen and co-workers[11] have fabricated square patterns of ZnO nanorods on four-inch thermoplastic poly(urethane) (TPU) surfaces via standard photolithography and etching processes. Such etching requires relatively complex multistep procedures for obtaining the desired ZnO patterns on the substrate surfaces and, moreover, the acidic condition would

[*] Dr. P. Yang, S. Zou, Prof. W. Yang
The State Key Laboratory of Chemical Resource Engineering
Beijing 100029 (P.R. China)

Dr. P. Yang, S. Zou, Prof. W. Yang
Department of Polymer Science
Beijing University of Chemical Technology
P.O. Box 37#, Beijing 100029 (P.R. China)
E-mail: yangwt@mail.buct.edu.cn

potentially damage certain reactive polymer substrates such as poly (ethylene terephthalate) (PET). In addition to etching, also direct ACG, based on patterned functionalized surfaces provided by hybrid SAM chemical structures, has potential in the fabrication of ZnO patterns. The reaction mechanism behind the ACG process can be summarized as the alkaline hydrolysis of a zinc cation according to Scheme 1.[28] A series of zinc salts have been essayed as the zinc cation source, and these include $Zn(CH_3COO)_2$ (I),[22] $Zn(NO_3)_2$ (II),[25,26] and $ZnF(OH)/Zn(Et)_2$ (III).[23,24] The OH^- source was provided by the zinc salt itself, for example, $Zn(Et)_2$ or a weak base such as NH_4F, ammonium, $(CH_2)_6N_4$ (HMT), or dimethylamine borane (DMAB). Researchers have found that changing the reaction system and the SAM chemical structure on surfaces would have a large and complex effect on the deposition. For (I) plus ammonium, Masuda et al.[22] have demonstrated that an alkyl-terminated surface favors the deposition of ZnO whereas a hydroxylated surface weakens it. However, van der Boom and Saito et al.[23,24] obtained the opposite results when using (III) and NH_4F. For (II) with HMT, Hsu et al.[25] reported that the carboxylated surface weakened the deposition and that ZnO nanorods would only grow selectively on a silver film uncovered by SAM; Gedanken and co-workers[26] showed that ordered ZnO crystals could be grown on silicon coated with phenyl-terminated SAMs. Saito et al.[17] expressed an alternative to direct ACG on SAM surfaces that consisted of first selectively attaching Pd catalyst particles onto the phenyl groups of a photopatterned SAM Si surface with phenyl/OH-terminated functionalities, after which a low-temperature (55 °C) ACG of ZnO was preferentially achieved on the Pd-enriched phenyl-terminated regions. Compared with etching, the SAM-based ACG process is easier to perform, and the control and tuning of the morphology of the ZnO particles are facilitated.

To the best of our knowledge, such a SAM-based ACG process has at present not been applied to functionalized polymer surfaces. A possible problem is the difficulty in modifying patterned surfaces of plastic substrates through the SAM method, since this approach is limited to metal and inorganic surfaces. For polymers, there exists only one good example constructed on a PET surface modified with 3-aminopropyltriethoxysilane (APTES) through an aminolysis reaction[29] to fabricate a silicalike surface, which could further initiate the grafting of SAM. However, there are no reports on a continuation of this work concerning patterned SAM and ZnO construction on such a surface.

A novel process that differs from the SAM method was recently developed to modify polymer surfaces. This process is known as confined photocatalytic oxidation (CPO).[30] In this reaction, sulfate anion (SO_4^-) groups could quickly be implanted in various polymer substrates including polyolefins,

$$(CH_2)_6N_4 + 6H_2O \longrightarrow 6HCHO + 4NH_3$$

$$NH_3 + H_2O \rightleftharpoons NH_4^+ + OH^-$$

$$2OH^- + Zn^{2+} \longrightarrow ZnO + H_2O$$

Scheme 1. The ACG reaction scheme.[28]

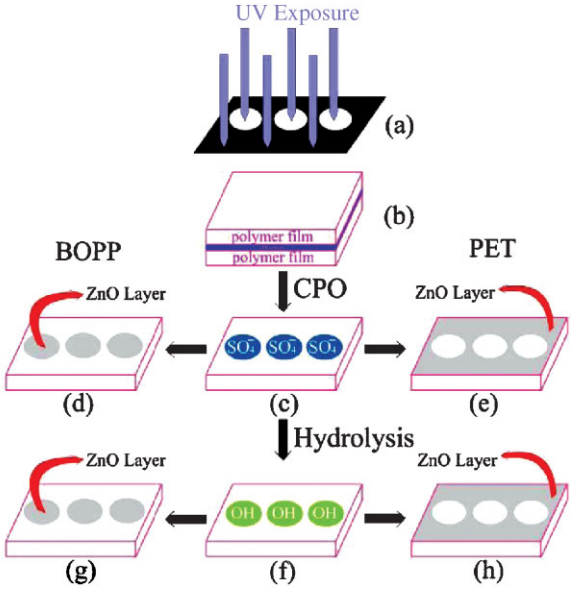

Figure 1. The growth scheme of the ZnO layer on patterned functionalized polymer surfaces: a) UV rays transported selectively through a photomask with circular holes; b) a sandwich setup consisting of two polymer films with a persulfate ammonium solution in the middle, irradiated by UV light whose route was controlled by the photomask; c) following the patterned irradiation, the sulfate groups could be selectively grafted onto the irradiated regions, which could be further transformed into hydroxyl groups by a hydrolysis reaction (f). The ZnO layer selectively remained on the sulfated and hydroxylated regions of the BOPP film (d, g), whereas for PET, the growth of the ZnO layer selectively remained on the unirradiated regions (e, h).

polyesters, nylons, and rubbers under UV irradiation. By using a photomask, the irradiation region could be controlled leading to a patterned, chemically functionalized surface being easily obtained. Moreover, the grafted sulfate groups were readily transformed into hydroxyl groups by a simple hydrolysis, which was clearly demonstrated and further used for initiating surface condensation polymerization on reactive sites.[31,32] In a series of research projects, we have found that for the fabrication of the films by chemical solution deposition, such patterned surfaces could be used as alternatives to SAM-modified surfaces with the advantage of this method being easily extended to various kinds of polymer substrates. Two examples include patterned organic macromolecules (polyaniline)[33] and inorganic materials (TiO_2)[32] that have been successfully fabricated on inert and reactive polymer surfaces. The present results constitute a first report on patterned ZnO ACG on polymer substrates modified by such a method. It was found that positive ZnO micropatterns were formed on sulfated and hydroxylated biaxially oriented poly(propylene) (BOPP) surfaces whereas, when using the same photomask and deposition conditions, negative patterns were obtained on sulfated and hydroxylated PET surfaces (Figure 1). The obtained ZnO film consisted mainly of vertical and parallel arrays of ZnO rods with diameters in the range of 500–750 nm and thicknesses of approximately 2–3 μm. Such thick wire arrays have displayed effective behaviors in solar cells, photocatalysis, lithium batteries, biomolecule detection,

NANO MICRO small

as well as optical and piezoelectric applications.[34] Finally, the formation mechanism of the positive and negative patterns was also investigated.

2. Results and Discussion

2.1. Positive Patterns on BOPP Substrates

When the patterned sulfated BOPP film was allowed to come into contact with the ACG reaction solution, the deposition occurred simultaneously on the irradiated/unirradiated regions without obvious deposition pattern being observed. The right image of Figure 2b showed that the deposition layer consisted of ZnO rods with a diameter of approximtely 680 nm. However, once the as-deposited film underwent an ultrasonic washing, the resulting film displayed a regular circular pattern where the ZnO layer remained only on the irradiated region, as shown in Figure 3a. A magnification of the micrograph in Figure 3b demonstrated that the diameter in the deposited region was about 40 μm, which approached the feature of the photomask. The cross-sectional shape of the ZnO pillar was typically hexagonal (Figure 3c) and the average diameter of the rods was ≈680 nm, that is, the same as before the ultrasonic washing. The peak positions of the X-ray diffraction (XRD) pattern (Figure 4a, lower curve) showed a good match with the standard pattern of a wurtzite ZnO crystal from the JCPDS database. The intensity at (002) was somewhat higher than that of a standard pattern of a randomly dispersed ZnO particle, suggesting an enhanced orientation effect of the pillar *c*-axis vertical to the substrate. As a result, the distribution density of the arrayed rods could be estimated as 0.8 μm^2 by counting the number of rods in Figure 3c. Furthermore, atomic force microscopy (AFM) measurements (Figure 3d) clearly described the typical character of the ZnO layer as the vertical growth of ZnO rods based on the deposited region. Height-profile analysis showed that the length of the ZnO rods (i.e., the thickness of ZnO layer) was near 2.5 μm.

The patterned hydroxylated BOPP surface also supported a positive pattern formation. As shown in Figure 5, after ultrasonic washing, vertical ZnO rods selectively remained on the hydroxylated BOPP regions. The average diameter of these rods was about 500 nm. The feature size of the circular pattern was 60 μm in diameter, in accordance with the size of the photomask (also 60 μm in diameter). The extent of pollution outside the irradiated regions was somewhat higher than that on the sulfated surfaces, showing a lower deposition selectivity than on the sulfated areas. Although the deposition selectivity decreased significantly, the orientation of the ZnO rods was found to be more regular than that of the sulfated surface. Most of the rods showed a uniform vertical growth from the underlying substrate (Figure 5b) with a higher distribution density (vide infra). Further XRD patterns (Figure 4a, upper curve) demonstrated that the dominating *c*-axis direction of the ZnO pillar was perpendicular to the substrate, since the diffraction peak at (002) dominated the whole pattern. The intensity at (002) increased drastically when the substrate changed from a sulfated to a hydroxylated BOPP surface, revealing highly enhanced vertical *c*-axis orientations on the hydroxylated substrate. Consequently, it was reasonable to calculate the pillar distribution density on the hydroxylated surface from scanning electron microscopy (SEM) pictures, rendering it possible to verify the possibility of controlling and adjusting the density along the surface. As shown in Figure 6, at a constant deposition time, the corresponding distribution density increased from 0.7 to 1.8 μm^{-2} when increasing the salt concentration from 0.1 to 0.2 M. On the other hand, the pillar density increased from 0.7 to 1.3 μm^{-2} when the deposition time was prolonged from 24 to 48 h with a constant salt concentration. The calculated results showed that doubling the salt concentration or deposition time would also double the pillar density. Therefore, these preliminary results demonstrated that the density of the vertical ZnO rods could be simply adjusted by changing the salt concentration and deposition time.

2.2. Negative Patterns on PET Substrates

The work described above demonstrated that positive ZnO micropatterns could be obtained on sulfated and hydroxylated BOPP surfaces, where the ZnO rods selectively remained on the functionalized (irradiated) regions. As a next step, similar experiments were conducted on a PET surface. PET is different from BOPP due to its chemical activity towards the surrounding environment. Initial results displayed a completely different path when performing such patterned depositions. As can be seen in Figures 7 and 8, after ultrasonic washing, the ZnO rods were surprisingly found to remain on the blank regions of the polymer instead of on the sulfated or hydroxylated regions, there forming a continuous ZnO network with ordered dispersed holes. The hole diameter was around 50 μm, that is, nearly 25% larger than the feature size of the photomask used

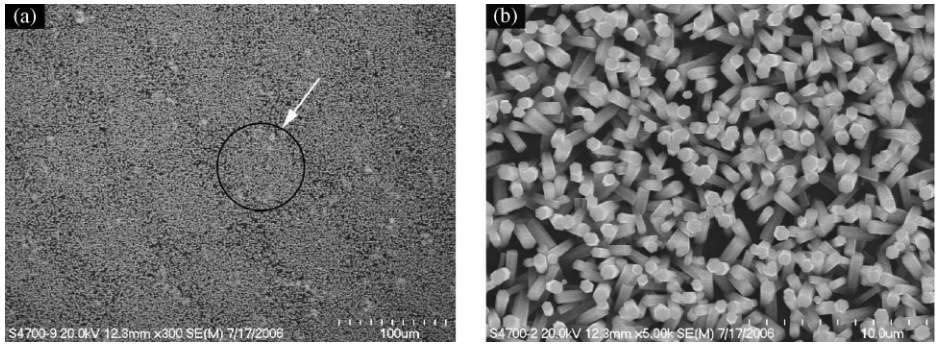

Figure 2. SEM micrographs of an as-deposited ZnO film on a patterned sulfated BOPP surface. As indicated by the circle and arrow in the left image, a very weak circular deposition pattern could be detected, which showed that the deposition did not display a direct selectivity without ultrasonic washing. The right image shows that the deposition layer consisted of arrayed ZnO rods with an average diameter of about 680 nm.

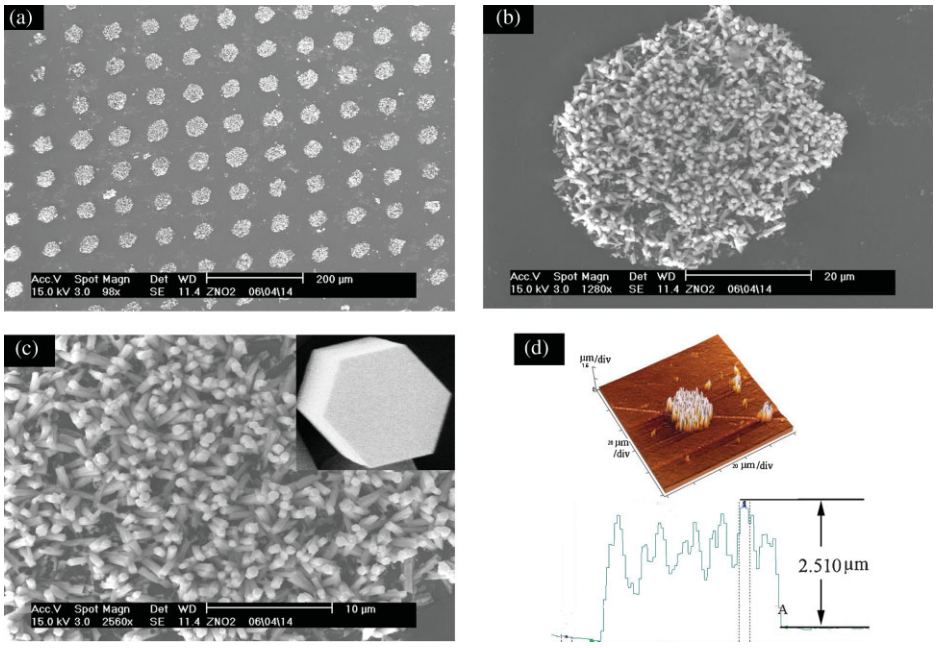

Figure 3. a–c) SEM and d) AFM images of a patterned ZnO deposition on a sulfated BOPP surface via ultrasonic washing. a) The resulting film showed a regular circle pattern where the ZnO layer could be found solely on the irradiated region. The magnifications (b, c) show that the diameter of the deposited region and a single ZnO pillar was about 40 μm and 680 nm, respectively. The cross-sectional shape of the ZnO pillar was typically hexagonal (inset picture in (c)). d) An AFM image of a single circular pattern indicated a thickness of the ZnO layer on the sulfated area of about 2.5 μm.

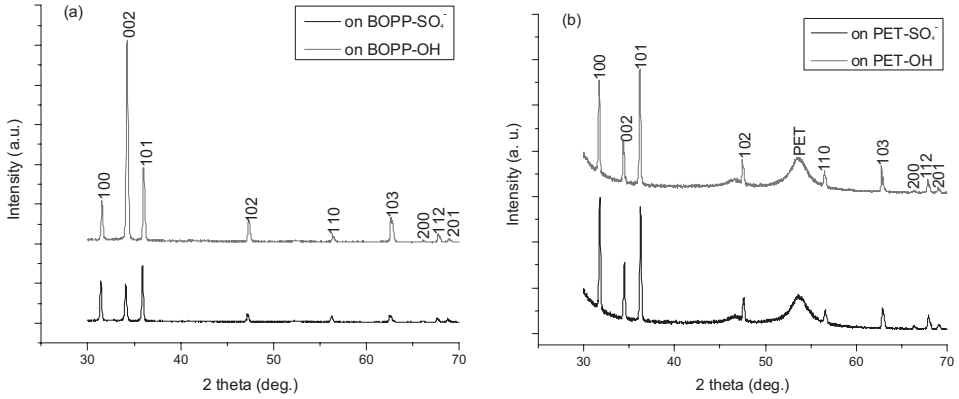

Figure 4. XRD patterns of ZnO rods deposited on substrates of a) sulfated BOPP (lower curve in (a), BOPP-SO_4^-), hydroxylated BOPP (upper curve in (a), BOPP-OH), and b) sulfated PET (lower curve in (b), PET-SO_4^-) and hydroxylated PET (upper curve in (b), PET-OH).

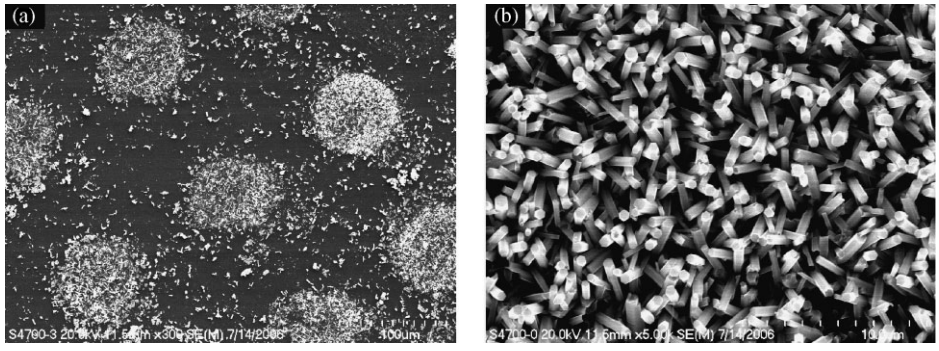

Figure 5. a) A SEM micrograph of a patterned ZnO deposition on a hydroxylated BOPP surface and b) a magnification of one circular region. By ultrasonic washing, the ZnO pillar became selective to the hydroxylated BOPP region whereas a few particles dispersed into the unirradiated region. The average diameter of the ZnO rods was 500 nm.

small NANO MICRO

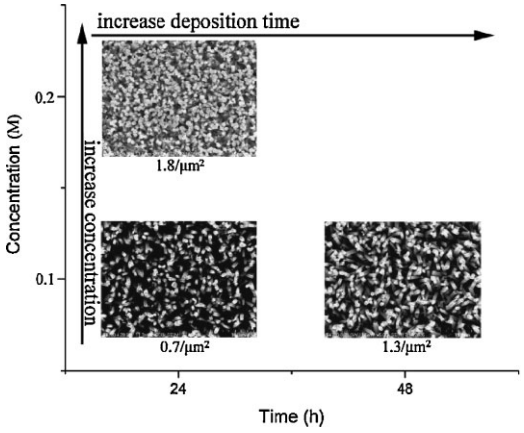

Figure 6. The effects of the deposition time (h) and reactant concentration (M) on the distribution density of ZnO rods on hydroxylated BOPP substrates. The pillar density (μm^{-2}) can be seen below each picture. All of the depositions were carried out at 90 °C.

(40 μm in the diameter). In both cases, the ZnO rods showed uniform size features: equivalent average diameters, nearly 750 nm, and lengths (i.e., film thickness) of 2.7 μm. Most of the rods tended to lie down on the substrate, which was in agreement with the results of the XRD analysis. From these XRD patterns (Figure 4b), low vertical *c*-axis orientations were observed on both PET substrates; alternatively, almost the same *c*-axis orientation parallel to the substrate, that is, the (100) peak, dominated the patterns. A clearer contrast between irradiated and unirradiated regions was observed on the hydroxylated surface (Figure 8a), which displayed a higher selective deposition than on the sulfated surface (Figure 7a).

2.3. Photoluminescence of ZnO Crystallites

The photoluminescence property of a ZnO crystal was also investigated. Near UV and visible luminescence from ZnO crystals were detected by fluorescence microscopy and spectroscopy (Figure 9). Strong UV and visible-light luminescence originated from band-edge emission (395 nm) and the oxygen vacancy (450–600 nm), respectively,[22,35] showing a potential for polymer-based display devices.

2.4. Pattern Formation Mechanism

The chemical solution growth of metal oxide on substrates mainly involves homogeneous and heterogeneous processes from supersaturated solutions. The latter is shown to be induced by terminated functional groups of SAM on the substrate surfaces.[8] The introduction of functionalities decreases the interfacial energy between the metal oxide and the surface, and accordingly, the deposition of ceramic films at a lower extent of supersaturation is facilitated. It has been reported that within

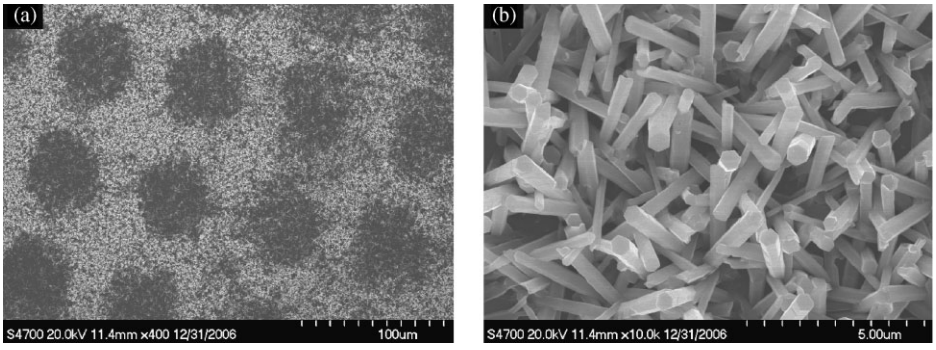

Figure 7. SEM micrographs of ZnO deposition on patterned sulfated PET surface and the magnification displaying the detailed deposition on sulfated (the dark regions in (a)) and unirradiated regions ((b) and the bright regions in (a)). Very little deposition was found on the sulfated regions represented by a circular pattern. Rather, the deposition was mainly found to form a continuous network on the unirradiated regions. The average diameter of the ZnO rods was about 750 nm.

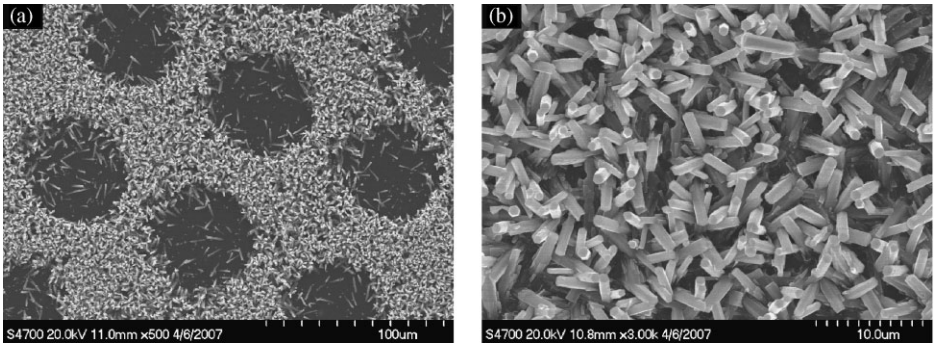

Figure 8. SEM micrographs of the ZnO deposition on a patterned hydroxylated PET surface and the magnification displaying the detailed deposition on hydroxylated (the dark regions in (a)) and unirradiated regions ((b) and the bright regions in (a)). The average diameter of ZnO rods was about 750 nm.

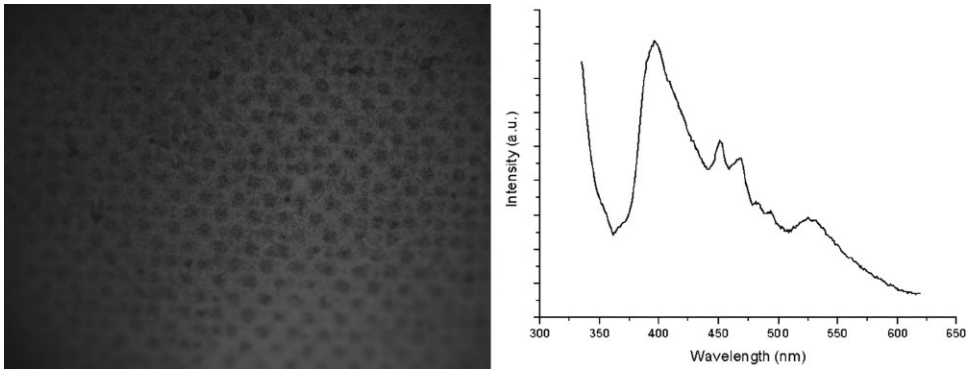

Figure 9. A photoluminescence image of a patterned ZnO deposition on a sulfated BOPP substrate under UV light illumination (365 nm). The corresponding emission spectra of ZnO deposition layer is shown in right picture (the excitation wavelength is 325 nm).

several hours, a SAM-modified surface could quickly induce heterogeneous nucleation and growth of ZnO at low temperature (50 °C).[22–26] The solution remained transparent during the whole reaction process, showing no obvious homogeneous nucleation. Similarly, attempts were made to utilize such a process on sulfated and hydroxylated polymer surfaces. As shown in Figure 10, the deposition on sulfated BOPP surface (50 °C for 1 h) showed a very weak pattern, obviously different from the encouraging results on SAM surfaces.[22–26] Therefore, it seemed to be impossible to apply a pure heterogeneous process to the sulfated and hydroxylated polymer surfaces fabricated by our method. This was reasonable since the density and regular extent of sulfate and hydroxyl groups were lower than SAM; for instance, the water-contact angle (WCA) of the hydroxylated BOPP surface was only 80°.[31,32] This value was much higher than that of a OH-terminated SAM surface,[22–24] indicating a lower OH density. As a result, these groups were unable to decrease the interfacial energy as effectively as SAM.

Alternatively, the temperature was increased to 90 °C and the deposition time to several tens of hours, which is usually a condition for homogeneous chemical solution growth.[36] More interference from the homogeneous process would result in a weak adhesion between the ZnO layer and the substrate, and thus weaken the role of the grafted functional groups. This could be reflected by the change of the deposition method. After the same deposition procedure, but when the substrate was soaked in the solution instead of being floated at the surface, a large part of the ZnO layer was peeled off by the ultrasonic washing, thus leaving only a weak negative pattern on the sulfated PET surface (Figure 11a). Therefore, the heterogeneous process must be deliberately enhanced at such conditions by eliminating the gravity-induced adsorption of particles from the solution. A functionalized substrate surface was floated on the solution surface, facing downwards, instead of being completely soaked in the solution. Such a procedure was found to effectively lower the adsorption of ZnO particles formed by the homogeneous process. As a result, a better pattern was obtained on the sulfated PET surface (Figure 11b).

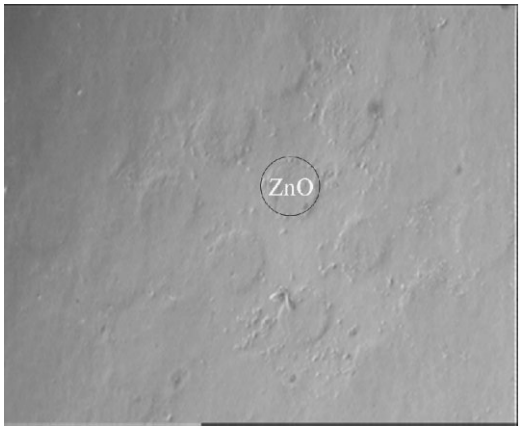

Figure 10. An optical image of a positive ZnO pattern on a sulfated BOPP surface at low temperature. The concentration of the salts was 0.1 M and the deposition time was 1 h at 50 °C.

The floating method rendered it possible to efficiently vary the effect of the interfacial functional groups on the deposition at a higher extent of supersaturation than in the SAM case. However, unlike the direct observation on the SAM surfaces, the effect in this system had to be presented by a post-washing treatment. For instance, Figure 2 showed that before washing, the deposition still displayed a poor selectivity, as a result of physisorption of ZnO particles on unirradiated regions. However, the functional-group-supported deposition could be seen once the as-deposited film undertook an ultrasonic washing step (Figures 3–8), demonstrating the difference in adhesion strength between the two regions. A detailed analysis made it possible to verify the effect of various groups on the deposition, much the same as the evaluation on different SAM surfaces.[22–26]

On BOPP substrates, functionalized sulfated and hydroxylated regions were found to favor the formation of a ZnO layer with a high bonding strength, and consequently this part of the layer could sustain during the ultrasonic peeling. In contrast, an unmodified surface had only saturated aliphatic carbon chains, which were able to support only a weak ZnO layer formation. Obviously, this could not resist the ultrasonic washing, and subsequently, positive ZnO patterns were formed where ZnO rods selectively arrayed on the functionalized BOPP surface. This suggestion was supported by the work by Ozkan et al. in their demonstration that sulfonate groups, which are similar to sulfates, could form an electrostatic co-ordination bonding with ZnO particle surfaces.[37] Our observations were also in agreement with those

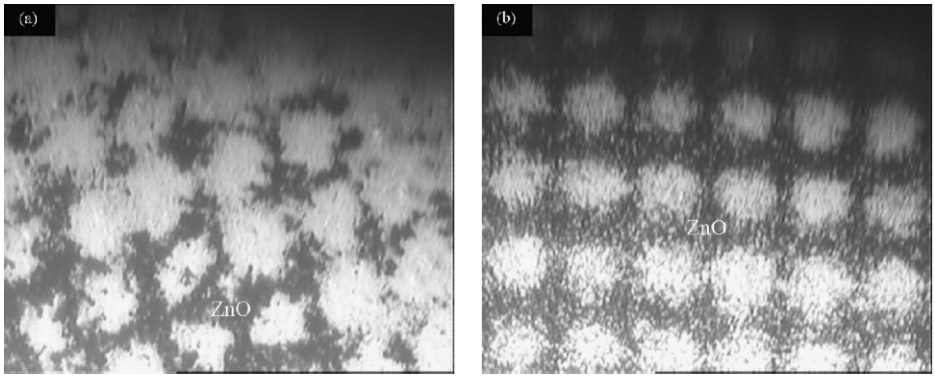

Figure 11. Optical images of negative patterns fabricated by two different methods: a) soaking the patterned sulfated PET film in the solution; b) floating the patterned sulfated PET film on the solution surface with the functionalized surface facing downwards.

reported by van der Boom and Saito et al.,[23,24] who showed that the growth of a ZnO film was facilitated on OH-terminated SAM surfaces. It is known that a side reaction to the grafting of sulfate groups in an aqueous environment can take place, transforming the sulfates into hydroxyl groups. A byproduct of this reaction is a proton (H^+).[30,38] This newly formed H^+ would decrease the extent of supersaturation of the solution as a result of a neutralization with OH^- formed by the hydrolysis of HMT. Accordingly, during the same time scale, the extent of reaction on the sulfated BOPP surface would be lower than that on the hydroxylated BOPP surface. Under equivalent conditions (0.1 M, 90 °C, 48 h), the density of the ZnO rods on a sulfated BOPP surface was 0.8 μm^{-2} (Figure 3c), whereas this value increased to 1.3 μm^{-2} on the hydroxylated surface (Figure 6). Another consequence of the higher reaction extent was that a larger amount of ZnO was physisorbed on the unirradiated regions neighboring the hydroxylated regions. This resulted in a larger amount of pollution outside the irradiated regions as compared to on the patterned sulfated BOPP surface. This was consistent with the SEM observations in Figures 3 and 5.

For the negative patterns on PET substrates, it was interesting to note that the deposition remained only on the unirradiated regions whatever the functional group on the irradiated regions was. Koumoto and co-workers[22] found that the ZnO layer grew selectively only on hydrophobic PET surfaces, and suggested that the ZnO crystal surface could become hydrophobic by the adsorption of certain hydrophobic organic molecules used in the solution. A high WCA (140°) was observed on a silicon substrate covered with many deposited ZnO crystals. Moreover, the WCA on a hydroxylated PET surface with ZnO depositions was found to be around 132°, further reflecting the hydrophobicity of the ZnO crystals. Consequently, the hydrophobic ZnO crystallites naturally preferred the hydrophobic unirradiated PET surface. This phenomenon was analyzed further from another point of view. As opposed to inert BOPP, PET is a relatively reactive substrate containing abundant ester bonds. These are capable of undergoing hydrolysis reactions in aqueous environments.[39] A related lesson was given by Pizem et al.,[40] who pointed out that during the solution deposition process of a titanium film, reactive imide groups could be

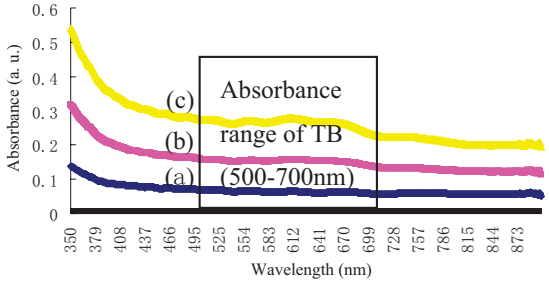

Figure 12. UV/Vis absorbance spectra of a) the blank PET along with two substrates after dying with TB: b) virgin PET, and c) sulfated PET surfaces. Before dying, the latter two surfaces were floated in an HMT solution (0.1 M) at 90 °C for 48 h.

partially hydrolyzed and thereby influence the deposition because of the acidic oxide deposition solution. Accordingly, the extent of hydrolysis of the sulfated and virgin PET substrates was first verified by floating them in HMT solution (0.1 M) without adding $Zn(NO_3)_2$. After being reacted at 90 °C for 48 h, the films were taken out and stained with toluidine blue (TB) to investigate the amount of carboxyl groups.[32,41] The amount of TB could be qualitatively evaluated by UV/Vis spectra where a wide peak between 500 and 700 nm was assigned to the molecular structure of TB.[42] In Figure 12, a higher absorbance intensity can be observed on the sulfated surface as compared to the virgin substrate, proving the presence of more COOH groups on the irradiated sulfated surface. From the molecular structure of the PET chain, it was easy to conclude that sulfate and hydroxyl groups could only be grafted onto the α site of the glycol ester ($COOCH_2$-CH_2OOC) because of free hydrogen atoms on this site. Polar α-substituted groups such as halogen and hydroxyl groups could effectively increase the rate constant of the alkaline

Table 1. Changes in pH during the ACG process for two types of PET surfaces.

	PET surfaces	
	Virgin PET	Sulfated PET
0	7.90	7.90
48 h	8.58	8.44

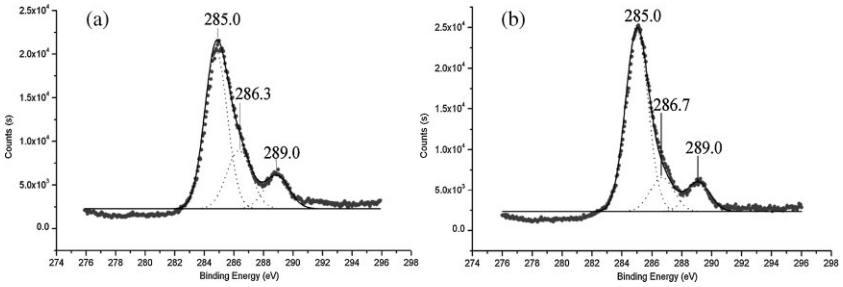

Figure 13. Carbon XPS spectra on a) sulfated and b) hydroxylated PET surfaces after the ACG process.

hydrolysis.[43] Consequently, the existence of polar sulfate and hydroxyl groups on irradiated PET regions would facilitate the alkaline hydrolysis to release COOH groups in a weak base environment, whereas this effect was not obvious on unirradiated regions without such polar groups. Evidence of such behavior was given by pH measurements (Table 1). The initial pH in the HMT solution was about 7.90, and after 48 h of hydrolysis at 90 °C, the solution in contact with the virgin PET substrate displayed a pH of 8.58. The pH of the solution in contact with the sulfated PET substrate, on the other hand, was 8.44. This lower pH reflected a higher extent of hydrolysis, and was due to a larger amount of acid hydrolysis products such as terephthalate salt[39] (NH_4^+-OOC-Φ-$COO^-NH_4^+$) being released into the solution. This speculation was strongly supported by XPS data (Figure 13). The carbon peak of the blank PET surface could be deconvoluted by curve fitting into three C_{1s} single core levels with assignments of 285.0 eV for the aromatic carbon, 286.5 eV for the carbon bearing a single oxygen (C–O), and 288.9 eV for the ester bond carbon (COO).[44] The change in concentration ratio of C (aromatic) to C-bearing oxygen atom [C(C–O) + C(COO)] could be used to evaluate the extent of hydrolysis. After the ACG process, the peak ratio of C (aromatic) to C (C–O + COO) on the sulfated PET surface was 61:39, whereas this value was 73:27 on the hydroxylated PET surface (Table 2).

By comparing both these values with the peak ratio on the virgin PET surface (obtained with the same ACG process), that is, 54:46, it was explicitly found that the total amount of C–O and COO decreased significantly after the implantation of polar groups. This in turn revealed that the content of ester bonds on the PET surface diminished noticeably. The extent of hydrolysis on the unirradiated regions was deduced to be very low, since the peak ratio, 54:46 on the virgin PET surface with the same ACG process, was close to that on the blank PET surface without any treatment (56:44). Moreover, the content of C–O and COO on the sulfated surface was higher than that on the hydroxylated surface, showing a higher extent of hydrolysis on the latter. This would lead to higher deposition selectivity on hydroxylated surfaces (vide infra).

Table 2. High-resolution XPS analysis on different PET surfaces.

Surface	Carbon (aromatic, %)	Carbon (C–O + COO, %)
Blank PET	57.5	42.5
Virgin PET (after ACG process)	53.92	46.08
Sulfated PET (after ACG process)	61.41	38.59
Hydroxylated PET (after ACG process)	72.78	27.22

One direct result from the hydrolysis reaction was the release of carboxyl groups. Negative patterns on a PET surface showed that COOH weakened the deposition of the ZnO layer as compared to ester chains on blank regions. A higher extent of hydrolysis resulted in the hydroxylated PET surface being able to more effectively suppress the deposition of ZnO than the sulfated surface. This was due to more carboxyl groups being released on the hydroxylated surface, and this played a key role in hindering the ZnO growth. As a result, the zinc concentration on a hydroxylated PET surface, as obtained by X-ray photoelectron spectroscopy (XPS) analysis, was nearly 0, whereas on a sulfated surface it increased to about 2%. This was also in accordance with the SEM observations, where the hydroxylated PET surface was found to have a higher deposition contrast than the sulfated PET surface (Figures 7 and 8). Such a role of COOH has been suggested and demonstrated by Hsu et al.,[25] who showed during the ACG process, COOH endgroups of SAM were first deprotonated and negatively charged. Instead of being attracted to the positively charged Zn growth species, negatively charged carboxyl groups preferentially bonded with HMT molecules, thus creating an effective electrostatic and/or steric block that inhibited the ZnO nucleation on the SAM. Accordingly, in our system, a similar behavior was believed to be responsible for the formation of negative patterns on the PET surfaces, demonstrating that the functionalized regions hindered the ZnO growth due to a larger amount of COOH groups than in the unirradiated regions.

3. Conclusions

In conclusion, a very simple method was developed to create positive and negative ZnO micropatterns on inert and reactive polymer surfaces. By ultrasonic washing, positive ZnO micropatterns could form on BOPP surfaces where the ZnO films selectively remained on the UV-exposed regions. Patterned ZnO films made up of vertical arrayed rods, typically 500 nm in diameter, could be fabricated on hydroxylated BOPP surfaces, and the pillar distribution density could be controlled by adjusting the salt concentration and deposition time. Sulfated BOPP surfaces supported the growth of mixed parallel and vertical ZnO rods with diameters around 680 nm. For hydroxylated and sulfated PET surfaces, ZnO rods, typically 750 nm in diameter, selectively remained on the unfunctionalized (unexposed) blank regions with the dominating orientation being parallel to the substrates, resulting in negative patterns. Hydrolysis reactions of the ester bonds of the functionalized PET surfaces were found to

small NANO MICRO

cause the regions enriched with sulfate and hydroxyl groups to transform into carboxyl group-enriched regions. The carboxyl groups were considered to be suppressing agents hindering the ZnO deposition.

The present work presents a photoresist-free and etching-free method for fabricating positive and negative ZnO patterns on a flexible substrate with great flexibility in design, thus rendering it possible to implant various applications of ZnO micro- and nanostructures onto more popular polymer substrates. The ZnO micropattern described here and the TiO_2 micropattern reported elsewhere[32] demonstrate that the modification and deposition method developed in our lab has a great potential of becoming a general approach for fabricating positive and negative micropatterns of metal oxide films on common plastic substrates without the use of standard photolithographic procedures. Moreover, such a method may possibly promote the development of patterned ceramic films on flexible organic polymeric substrates, which is a hot demand in modern materials science and engineering.[8]

4. Experimental Section

Materials: Commercially available BOPP and PET films were ultrasonically washed (80 kHz, with a 100% input power of 250 W) for 15 min in a sequence of water, ethanol, and acetone, and then dried in an oven before the subsequent modification. Ammonium persulfate (APS, analytical grade), zinc nitrate hydrate ($Zn(NO_3)_2 \cdot 6H_2O$, chemical grade), and hexomethylenetetramine (HMT, analytical grade) were used as received. Ultrapure water obtained from Aquapro (Shanghai, P.R. China) was utilized in all experiments.

Preparation of patterned sulfated polymer surfaces: A thin layer of an aqueous APS solution (30 wt %) was sandwiched between two polymer films (BOPP as the top film, and either BOPP or PET as the bottom film) and exposed to UV irradiation (high-pressure mercury lamp, 1000 W; UV intensity, 8000 $\mu m\ cm^{-2}$; irradiation time, 120 s). A photomask with a circular pattern was applied on the top film (Figure 1a) to control the irradiation region. Subsequently, the film was withdrawn and washed with water and acetone, after which it was dried in an oven (50 °C) for 5 min. A detailed description of this procedure can be found elsewhere.[30–33]

Preparation of patterned hydroxylated polymer surfaces: A hydrolysis reaction was conducted by floating the patterned sulfated film in ultrapure water at 30 °C for 13 h or more (with the sulfated surface facing downwards). After the reaction, the film was withdrawn and washed with water and acetone, respectively, after which it was dried in an oven (50 °C) for 5 min.

ZnO micropatterning on functionalized polymer surfaces: The fabrication process for the micropatterning is depicted in Figure 1. Firstly, a photomask was applied on the top BOPP film (Figure 1a) and patterned UV irradiation was carried out on the two polymer films with the persulfate ammonium solution sandwiched between them (Figure 1b). After a certain time, sulfate groups were implanted solely in the irradiated regions (blue regions, Figure 1c), and a hydroxylated surface could be easily obtained by the hydrolysis of these sulfated areas (Figure 1f). The patterned functionalized films (Figures 1c and f) were allowed to float in a solution containing a given amount of $Zn(NO_3)_2$ and HMT (with the modified surface facing downwards). Unless specifically mentioned, the deposition conditions included the use of equimolar salts (0.1 M) and a deposition at 90 °C for 48 h. Subsequently, the film was taken out and washed ultrasonically in distilled water for 20 min (80 kHz, with a 100% input power of 250 W). By employing such a process, ZnO rods could selectively remain on the sulfated and hydroxylated BOPP regions thus giving rise to positive patterns (as shown in Figure 1d and g, where the gray parts grew within the blue and green regions). For PET, on the other hand, the ZnO rods selectively remained on the unirradiated region providing negative patterns (as shown in Figure 1e and h, where the gray parts grew on the unirradiated surfaces).

Characterization: Optical microscopy observations were carried out on a Nikon TE2000-s system (Tokyo, Japan). AFM in tapping-mode was performed on a CP-II (DI Co., US). High-resolution field-emission SEM (FE-SEM) was conducted on Sterscan 250MK3 (Cambridge, UK) and HITACH 4700 (Japan). Surface contact-angle measurements were performed on an OCA 20 (Dataphysics, Germany). XPS spectra were obtained by using an ESCALAB 250 (VG Scientific) instrument and AlKα excitation at a 45° angle. UV/Vis absorption spectra were recorded by a GBC Cintra 20 spectrophotometer (Australia) and XRD analysis was carried out on a D/MAX 2500 VB2+/PC (Rigaku Co., Japan). Confocal fluorescent microscopy was performed with an Olympus IX71 (Japan), and the excitation UV (365 nm) intensity is 113 mW cm^{-2}. Fluorescence spectra were collected on HITACH F-4500FL ($\lambda_{exc} = 325$ nm).

Acknowledgements

The authors acknowledge funding of the Major Project (50433040) from the National Natural Science Foundation of China (NSFC) and the Major Project (XK100100433) for Polymer Chemistry and Physics Subject Construction from the Beijing Municipal Education Commission (BMEC).

[1] a) V. Djara, J. C. Bernéde, *Thin Solid Films* **2005**, *493*, 273; b) T. Shirakawa, T. Umeda, Y. Hashimoto, A. Fujii, K. Yoshino, *J. Phys. D: Appl. Phys.* **2004**, *37*, 847.

[2] a) J. Wöllensteina, J. A. Plazab, C. Canéb, Y. Minc, H. Böttnera, H. L. Tuller, *Sens. Actuators B* **2003**, *93*, 350; b) K. D. Mitzner, J. Sternhagen, D. W. Galipeau, *Sens. Actuators B* **2003**, *93*, 92; c) H. K. Hong, H. W. Shin, H. S. Park, D. H. Yun, C. H. Kwon, K. Lee, S. T. Kim, T. Moriizumi, *Sens. Actuators B* **1996**, *33*, 68.

[3] K. C. Hui, C. W. Lai, H. C. Ong, *Thin Solid Films* **2005**, *483*, 222.

[4] a) J. Goldberger, D. J. Sirbuly, M. Law, P. Yang, *J. Phys. Chem.* **2005**, *109*, 9; b) K. Lee, J. H. Kim, S. Ima, *Appl. Phys. Lett.* **2006**, *88*, 023504.

[5] S. G. Girol, T. Strunskus, M. Muhler, C. Wöll, *J. Phys. Chem. B* **2004**, *108*, 13736; a) F. Boccuzzi, A. Chiorino, S. Tsubota, M. Haruta, *J. Phys. Chem.* **1996**, *100*, 3625.

[6] L. Guedri-Knani, J. L. Gardette, M. Jacquet, A. Rivaton, *Surf. Coat. Technol.* **2004**, *180–181*, 71.

[7] a) A. B. Djurišic, Y. H. Leung, *Small* **2006**, *2*, 944; b) S. J. Pearton, D. P. Norton, F. Ren, *Small* **2007**, *3*, 1144; c) N. Izyumskaya, V. Avrutin, U. Özgür, Y. I. Alivov, H. Morkoç, *Phys. Stat. Sol. B* **2007**, *244*, 1439.
[8] B. C. Bunker, P. C. Rieke, B. J. Tarasevich, A. A. Campbell, G. E. Fryxell, G. L. Graff, L. Song, J. Liu, J. W. Virden, G. L. McVay, *Science* **1994**, *264*, 48.
[9] a) M. Fu, J. Zhou, Q. Xiao, B. Li, R. Zong, W. Chen, J. Zhang, *Adv. Mater.* **2006**, *18*, 1001; b) Y. W. Koh, M. Lin, C. K. Tan, Y. L. Foo, K. P. Loh, *J. Phys. Chem. B* **2004**, *108*, 11419; c) S. H. Lee, H. J. Lee, D. Oh, S. W. Lee, H. Goto, R. Buckmaster, T. Yasukawa, T. Matsue, S. K. Hong, H. C. Ko, M. W. Cho, T. Yao, *J. Phys. Chem. B* **2006**, *110*, 3856; d) L. K. The, K. H. Yeo, C. C. Wong, *Appl. Phys. Lett.* **2006**, *89*, 051105.
[10] M. Kreye, B. Postels, H. H. Wehmann, D. Fuhrmann, A. Hangleiter, A. Waag, *Phys. Stat. Sol. C* **2006**, *3*, 992.
[11] T. Y. Liu, H. C. Liao, C. C. Lin, S. H. Hu, S. Y. Chen, *Langmuir* **2006**, *22*, 5804.
[12] S. W. Kim, M. Ueda, T. Kotani, S. Fujita, S. Fujita, *Phys. Stat. Sol. C* **2004**, *1*, 896.
[13] K. Takahashi, H. Funakubo, N. Ohashi, H. Haneda, *Thin Solid Films* **2005**, *486*, 42.
[14] S. J. Pearton, D. P. Norton, *Plasma Process. Polym.* **2005**, *2*, 16.
[15] Y. Tak, K. Yong, *J. Phys. Chem. B* **2005**, *109*, 19263.
[16] J. Y. Lee, D. Yin, S. Horiuchi, *Chem. Mater.* **2005**, *17*, 5498.
[17] a) N. Saito, H. Haneda, K. Koumoto, *Microelectron. J.* **2004**, *35*, 349; b) N. Saito, H. Haneda, T. Sekiguchi, N. Ohashi, I. Sakaguchi, K. Koumoto, *Adv. Mater.* **2002**, *14*, 418.
[18] H. He, Jr. J. H. Hsu, C. W. Wang, H. N. Lin, L. J. Chen, Z. L. Wang, *J. Phys. Chem. B* **2006**, *110*, 50.
[19] X. Wang, C. J. Summers, Z. L. Wang, *Nano Lett.* **2004**, *4*, 423.
[20] A. Dorfman, N. Kumar, J. Hahm, *Langmuir* **2006**, *22*, 4890.
[21] J. Rybczynski, D. Banerjee, A. Kosiorek, M. Giersig, Z. F. Ren, *Nano Lett.* **2004**, *4*, 2037.
[22] Y. Masuda, N. Kinoshita, F. Sato, K. Koumoto, *Cryst. Growth Design* **2006**, *6*, 75.
[23] T. Zubkov, A. B. Lucassen, D. Freeman, Y. Feldman, S. R. Cohen, G. Evmenenko, P. Dutta, M. E. van der Boom, *J. Phys. Chem. B* **2005**, *109*, 14144.
[24] N. Saito, H. Haneda, W. S. Seo, K. Koumoto, *Langmuir* **2001**, *17*, 1461.
[25] J. W. P. Hsu, Z. R. Tian, N. C. Simmons, C. M. Matzke, J. A. Voigt, J. Liu, *Nano Lett.* **2005**, *5*, 83.
[26] R. Turgeman, O. Gershevitz, O. Palchik, M. Deutsch, B. M. Ocko, A. Gedanken, C. N. Sukenik, *Cryst. Growth Design* **2004**, *4*, 169.
[27] M. Yan, Y. Koide, J. R. Babcock, P. R. Markworth, J. A. Belot, T. J. Marks, R. P. H. Chang, *Appl. Phys. Lett.* **2001**, *79*, 1709.
[28] Q. Li, V. Kumar, Y. Li, H. Zhang, T. J. Marks, R. P. H. Chang, *Chem. Mater.* **2005**, *17*, 1001.
[29] A. Y. Fadeev, T. J. McCarthy, *Langmuir* **1998**, *14*, 5586.
[30] P. Yang, J. Y. Deng, W. Yang, *Polymer* **2003**, *44*, 7157.
[31] H. Zhao, P. Yang, J. Deng, L. Liu, J. Zhu, Y. Sui, J. Lu, W. Yang, *Langmuir* **2007**, *23*, 1810.
[32] P. Yang, M. Yang, S. Zou, J. Xie, W. Yang, *J. Am. Chem. Soc.* **2007**, *129*, 1541.
[33] P. Yang, J. Xie, W. Yang, *Macromol. Rapid Comm.* **2006**, *27*, 418.
[34] a) H. J. Fan, W. Lee, R. Hauschild, M. Alexe, G. L. Rhun, R. Scholz, A. Dadgar, K. Nielsch, H. Kalt, A. Krost, M. Zacharias, U. Gösele, *Small* **2006**, *2*, 561; b) A. Dorfman, N. Kumar, J. Hahm, *Adv. Mater.* **2006**, *18*, 2685.
[35] a) X. L. Wu, G. G. Siu, C. L. Fu, H. C. Ong, *Appl. Phys. Lett.* **2001**, *78*, 2285; b) J. S. Kang, H. S. Kang, S. S. Pang, E. S. Shim, S. Y. Lee, *Thin Solid Films* **2003**, *443*, 5.
[36] a) L. Vayssieres, K. Keis, A. Hagfeldt, S. E. Lindquist, *Chem. Mater.* **2001**, *13*, 4395; b) L. Vayssieres, K. Keis, S. E. Lindquist, A. Hagfeldt, *J. Phys. Chem. B* **2001**, *105*, 3350; c) L. Vayssieres, *Adv. Mater.* **2003**, *15*, 464; d) Z. R. Tian, J. A. Voigt, J. Liu, B. Mckenzie, M. J. Mcdermott, *J. Am. Chem. Soc.* **2002**, *124*, 12954.
[37] S. Chaudhary, H. J. Kim, K. V. Singh, M. Ozkan, *Nano Lett.* **2004**, *4*, 2415.
[38] a) D. A. House, *Chem. Rev.* **1962**, *62*, 185; b) W. K. Wilmarth, A. Haim, in *Peroxide Reaction Mechanism*, (Ed: J. O. Edwards), Wiley Interscience, New York **1962**, p. 175; c) C. H. Bamford, G. K. Al-Lamee, *Polymer* **1994**, *35*, 2844.
[39] G. P Karayannidis, D. S. Achilias, *Macromol. Mater. Eng.* **2007**, *292*, 128.
[40] H. Pizem, O. Gershevitz, Y. Goffer, A. A. Frimer, C. N. Sukenik, U. Sampathkumaran, X. Milhet, A. McIlwain, M. R. De Guire, M. A. B. Meador, J. K. Sutter, *Chem. Mater.* **2005**, *17*, 3205.
[41] Y. Wang, H.-H. Lai, M. Bachman, C. E. Sims, G. P. Li, N. Allbritton, *Anal. Chem.* **2005**, *77*, 7539.
[42] a) L. D'Ilario, A. Martinelli, *Model. Simul. Mater. Sci. Eng.* **2006**, *14*, 581; b) D. D. Schlereth, H. L. Schmidt, *J. Electroanal. Chem.* **1995**, *380*, 117.
[43] a) G. Schmeer, S. Riembauer, J. Barthel, *J. Solution Chem.* **1990**, *19*, 1175; b) T. C. Bruice, T. H. Fife, *Tetrahedron Lett.* **1961**, *8*, 263; c) T. C. Bruice, T. H. Fife, *J. Am. Chem. Soc.* **1974**, *84*, 1973.
[44] a) E. Uchida, Y. Uyama, H. Zwata, Y. Ikada, *J. Polym. Sci. Part A: Polym. Chem.* **1990**, *28*, 2837; b) P. Yang, X. Zhang, B. Yang, H. Zhao, J. Chen, W. Yang, *Adv. Funct. Mater.* **2005**, *15*, 1415.

Received: September 17, 2007
Revised: March 10, 2008

